

Detection of precursor charge-density-wave order in $2H\text{-NbSe}_2$ by μSR

C. Gomez,¹ D. Braam,¹ S. Tezok,¹ and J.E. Sonier,^{1,2}

¹*Department of Physics, Simon Fraser University, Burnaby, British Columbia V5A 1S6, Canada*

²*Canadian Institute for Advanced Research, Toronto, Ontario M5G 1Z8, Canada*

(Dated: August 7, 2018)

We demonstrate the sensitivity of transverse-field muon spin rotation (TF- μSR) to static charge-density-wave (CDW) order in the bulk of $2H\text{-NbSe}_2$. In the presence of CDW order the quadrupolar interaction of the ^{93}Nb nuclei with the local electric-field gradient is modified, and this in turn affects the magnetic dipolar coupling of the positive muon to these nuclei. For a weak magnetic field applied parallel to the c -axis, we observe a small enhancement of the muon depolarization rate at temperatures below the established CDW phase transition. Aligning the applied field perpendicular to the c -axis, we observe a sensitivity to static CDW order in regions of the sample extending up to nearly 3 times the CDW transition temperature (T_0). The results suggest that the muon is mobile over the temperature range explored above the superconducting transition temperature (T_c), and becomes trapped in the vicinity of defects.

PACS numbers: 71.45.Lr, 74.70.Ad, 76.75.+i

I. INTRODUCTION

There is currently much interest in the interplay of CDW and superconducting states, driven by the discovery of short-range CDW correlations in the pseudogap phase of cuprates.^{1–7} Upon lowering the temperature the CDW correlation volume expands, but a reversal of this trend below T_c indicates a clear competition of the CDW order with superconductivity. Competing CDW order and superconductivity has also been demonstrated in the transition-metal dichalcogenide $2H\text{-NbSe}_2$,⁸ which like the cuprates is quasi two-dimensional. With decreasing temperature, $2H\text{-NbSe}_2$ undergoes an incommensurate CDW transition at $T_0 \sim 33$ K and becomes superconducting below $T_c \sim 7$ K.⁹ In contrast with cuprates, superconductivity in $2H\text{-NbSe}_2$ does not coexist with magnetism or lie in close proximity to a magnetic phase, and is mediated by a conventional electron-phonon interaction.

The occurrence of a long-range CDW state in $2H\text{-NbSe}_2$ for an extensive range of temperature above T_c differs from the situation in cuprates, where only short-range CDW correlations are observed above T_c . On the other hand, ^{93}Nb nuclear magnetic resonance (NMR) measurements show pre-translational broadening of quadrupolar transitions below $T \sim 75$ K, which has been attributed to precursor CDW fluctuations.^{10–12} Berthier *et al.* proposed that the CDW fluctuations inferred from the NMR measurements are induced near impurities,¹² which bears some resemblance to a more recent proposal by Tacon *et al.* that CDW correlations in cuprates are pinned in nanometer-size regions by lattice defects.¹³ More recently, nanodomains of static CDW order have been observed near defects in $2H\text{-NbSe}_2$ at temperatures $T_0 < T < 100$ K by scanning tunneling microscopy (STM).¹⁴ Intercalating $2H\text{-NbSe}_2$ with Co or Mn ions reduces T_0 , but short-range CDW order is found to persist for an extensive range of temperature above T_0 .¹⁵

The short-lived (with a mean lifetime of approximately

$2.2 \mu\text{s}$), spin $S = 1/2$, positive muon (μ^+) is most often used in condensed matter physics as a pure local magnetic probe, since it does not possess an electric quadrupole moment. However, magnetic dipolar coupling to quadrupolar nuclei provides an indirect sensitivity of the μ^+ to CDW correlations in the bulk. In $2H\text{-NbSe}_2$ the spin of the implanted μ^+ dipolar couples to the ^{93}Nb and ^{77}Se nuclear magnetic moments. The ^{93}Nb nuclei have spin $I^{\text{Nb}} = 9/2$ and possess an electric quadrupole moment (^{77}Se , which has nuclear spin $I^{\text{Se}} = 1/2$, does not), which interacts with the local electric-field gradient (EFG). In the presence of an applied static magnetic field \mathbf{B}_0 , both the μ^+ and ^{77}Se spins precess around \mathbf{B}_0 , the direction of which serves as a suitable quantization axis. On the other hand, the quantization axis for the ^{93}Nb nuclear spins is oriented along the vector sum of \mathbf{B}_0 and the direction of the maximal local EFG.

In a TF- μSR experiment, where the applied magnetic field \mathbf{B}_0 (chosen to be along the z direction) is perpendicular to the initial muon spin polarization $\mathbf{P}(0)$ (chosen here to be along the x direction), the time evolution of the muon spin polarization for $2H\text{-NbSe}_2$ is well described by

$$\begin{aligned} P_x(t) &= \exp(-\sigma^2 t^2) \cos(\gamma_\mu B_\mu t + \phi) \\ &= \exp[-(\sigma_{\text{Nb}}^2 + \sigma_{\text{Se}}^2) t^2] \cos(\gamma_\mu B_\mu t + \phi), \end{aligned} \quad (1)$$

where γ_μ is the muon gyromagnetic ratio, B_μ is the mean magnetic field sensed by the muon ensemble, ϕ is a phase constant, and σ_{Nb} (σ_{Se}) is the Gaussian depolarization rate associated with the dipolar coupling of the μ^+ to the ^{93}Nb (^{77}Se) nuclei. The muon depolarization rates are related to the width of the distribution of nuclear dipole fields in the z direction at the μ^+ site via the relation $\sigma^2 = \gamma_\mu \langle B_{\mu,z}^2 \rangle$, and are given by

$$\sigma_{\text{Se}}^2 = \frac{1}{3} \gamma_\mu^2 \gamma_{\text{Se}}^2 \hbar^2 I^{\text{Se}} (I^{\text{Se}} + 1) \sum_i \frac{(1 - 3 \cos^2 \theta_i)}{r_i^6} \quad (2)$$

and,¹⁶

$$\sigma_{\text{Nb}}^2 = \gamma_{\mu}^2 \gamma_{\text{Nb}}^2 \hbar^2 \sum_j \left\langle \left(\langle I_z^{\text{Nb}} \rangle_j \frac{(1-3\cos^2\theta_j)}{r_j^3} - \langle I_x^{\text{Nb}} \rangle_j \frac{3\sin\theta_j \cos\theta_j}{r_j^3} \right)^2 \right\rangle_{\text{av}}. \quad (3)$$

Here γ_{Se} (γ_{Nb}) is the gyromagnetic ratio of the ^{77}Se (^{93}Nb) nuclei, r_i (r_j) the distance between the μ^+ and the i^{th} ^{77}Se (j^{th} ^{93}Nb) nucleus, θ_i (θ_j) is the angle between \mathbf{B}_0 and the straight line connecting the μ^+ spin and the i^{th} ^{77}Se (j^{th} ^{93}Nb) nuclear spin, $I^{\text{Se}} = 1/2$ is the nuclear spin of ^{77}Se , $\langle I_z^{\text{Nb}} \rangle_j$ and $\langle I_x^{\text{Nb}} \rangle_j$ are the expectation values of the ^{93}Nb nuclear spin parallel and perpendicular to the z direction, and $\langle \rangle_{\text{av}}$ is the average over all eigenstates of the j^{th} ^{93}Nb nuclear spin. Note that in addition to the static spin component $\langle I_z^{\text{Nb}} \rangle_j$ parallel to \mathbf{B}_0 , the quadrupole interaction of the ^{93}Nb with the local EFG results in a static spin component $\langle I_x^{\text{Nb}} \rangle_j$ perpendicular to \mathbf{B}_0 . The second term in Eq. (3) then represents the contribution of this perpendicular static spin component to the dipole field in the z direction at the μ^+ site. Since the natural abundance of ^{77}Se is only $\sim 7.6\%$, the dipolar interaction with the ^{93}Nb nuclei dominates the depolarization of the TF- μSR spectrum.

The ratio $\langle I_x^{\text{Nb}} \rangle_j / \langle I_z^{\text{Nb}} \rangle_j$ depends on the ratio of the quadrupolar and Zeeman interaction energies. For strong magnetic field the Zeeman interaction of the ^{93}Nb spin with \mathbf{B}_0 dominates and the quantization axis of the ^{93}Nb nuclear spins is along the z direction. In this case $\langle (\langle I_x^{\text{Nb}} \rangle_j)^2 \rangle_{\text{av}} = 0$ and $\langle (\langle I_z^{\text{Nb}} \rangle_j)^2 \rangle_{\text{av}} = I(I+1)/3$, which reduces Eq. (3) to an equation analogous to Eq. (2). Of interest here is the situation at sufficiently low fields, where the magnitude of the quadrupolar interaction of the ^{93}Nb nuclei with the local EFG exceeds or becomes comparable to the Zeeman interaction. The quadrupolar coupling constant for ^{93}Nb in $2H\text{-NbSe}_2$ above T_0 is $e^2qQ/h \sim 62$ MHz,¹² and hence the ^{93}Nb quadrupolar frequency is $\nu_Q = 3e^2qQ/h2I(2I-1) \sim 2.58$ MHz. Consequently, the Zeeman and quadrupolar interaction energies are equivalent when the Zeeman frequency is $\nu_Z = 2.58$ MHz, which corresponds to a magnetic field of magnitude $B_0 = 2\pi\nu_Z/\gamma_{\text{Nb}} = 2.47$ kG. The EFG at the ^{93}Nb nuclear site in $2H\text{-NbSe}_2$ is due to the non-cubic ionic crystal lattice, but is modified by the presence of the μ^+ and its screening charge, and by the development of CDW correlations.

Since the μSR technique does not require the application of a magnetic field, greater sensitivity of the μ^+ to CDW order may be achieved by removal of the Zeeman interaction. However, the zero-field (ZF) μSR spectra for $2H\text{-NbSe}_2$ are rather complex. Higemoto *et al.* showed that the ZF- μSR signals fit well to a two-component dynamical Kubo-Toyabe function, but the physical interpretation of the various fit parameters are ambiguous.¹⁷ Here we show via TF- μSR measurements of $2H\text{-NbSe}_2$ that the complexity of the ZF- μSR spectra are the result of muon diffusion. Unlike the situation for zero field,

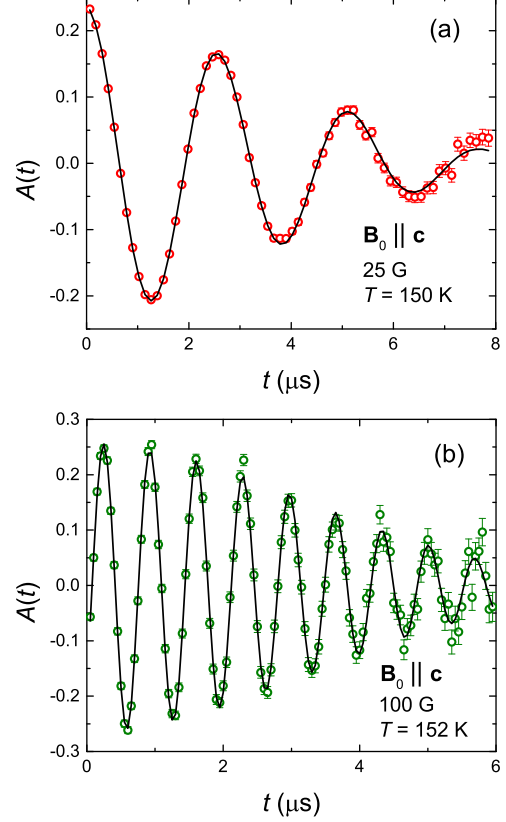


FIG. 1: (Color online) Representative TF- μSR spectra recorded at a temperature near 150 K and for a magnetic field of (a) 25 G, and (b) 100 G applied parallel to the c axis of $2H\text{-NbSe}_2$. The solid curves through the data points are fits to Eq. (4).

the TF- μSR signals are well described by a simple single-component depolarization function, which greatly simplifies the interpretation of the data.

II. EXPERIMENTAL DETAILS

Our TF- μSR experiments were carried out on a previously studied single crystal of $2H\text{-NbSe}_2$,¹⁸ which has a superconducting transition temperature of $T_c = 7.0$ K and an upper critical magnetic field of $B_{c2} = 45$ kG. The LAMPF and HELIOS spectrometers were used on the M20 surface μ^+ beam line at TRIUMF in Vancouver, Canada. The sample was mounted with the c axis parallel to the μ^+ -beam linear momentum. The majority of the measurements were performed with the applied magnetic field \mathbf{B}_0 parallel to the c axis, since the Lorentz force exerted by a perpendicular field causes deflection of the muon beam. Consequently, measurements with \mathbf{B}_0 perpendicular to the c axis were limited to the applied field strength of 25 G. In all cases the initial muon spin

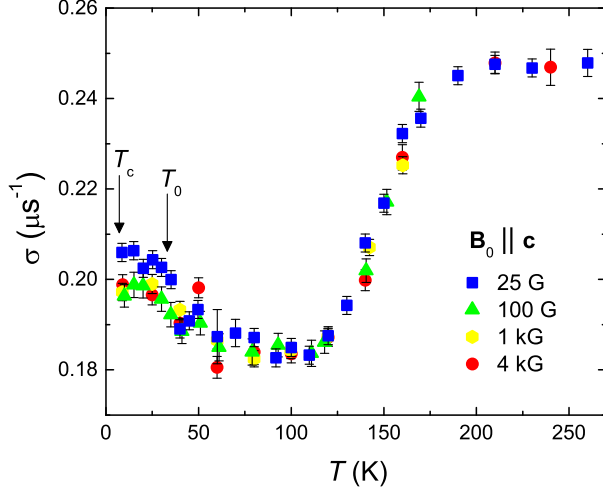


FIG. 2: (Color online) Temperature dependence of the muon depolarization rate σ above T_c for a magnetic field applied parallel to the c axis. The data for different magnetic field strengths have been vertically shifted to overlap above $T = 100$ K.

polarization $\mathbf{P}(0)$ was oriented perpendicular to \mathbf{B}_0 .

The TF- μ SR spectra were fit to

$$A(t) = a_s P(t) + a_b \exp(-\sigma_b^2 t^2 / 2) \cos(\gamma_\mu B_0 t + \varphi), \quad (4)$$

where a_s and a_b are the initial amplitudes of the sample and background signals, $P(t)$ is as defined in Eq. (1), and σ_b and φ are the muon depolarization rate and phase constant of the background component associated with muons that stop elsewhere outside the sample. The fits to Eq. (4) were performed assuming σ_b and the ratio a_s/a_b do not change with temperature. Examples of TF- μ SR spectra and the fits are shown in Fig. 1.

III. RESULTS AND DISCUSSION

Figure 2 shows the temperature dependence of the depolarization rate σ above T_c for different magnetic fields applied parallel to the c axis ($\mathbf{B}_0 \parallel \mathbf{c}$). There is some variation of σ with the applied field strength due to some uncertainty in determining the size of the background signal, which has a mean precession frequency close to that of the sample signal. Consequently, the data sets for different fields have been vertically shifted in Fig. 2 to overlap above $T = 100$ K, where CDW correlations are not expected. The ratio of the quadrupolar and Zeeman interaction energies of the ^{93}Nb nuclei for $B_0 = 25$ G, 100 G, 1 kG, and 4 kG are $\nu_Q/\nu_Z = 99, 25, 2.5,$ and 0.6 respectively. Hence the quadrupolar interaction is relevant to a varying degree for all magnetic fields considered in our experiments.

The strong temperature dependence of σ is indicative of thermally-activated hopping of the μ^+ . With increasing temperature σ first decreases, likely due to the μ^+

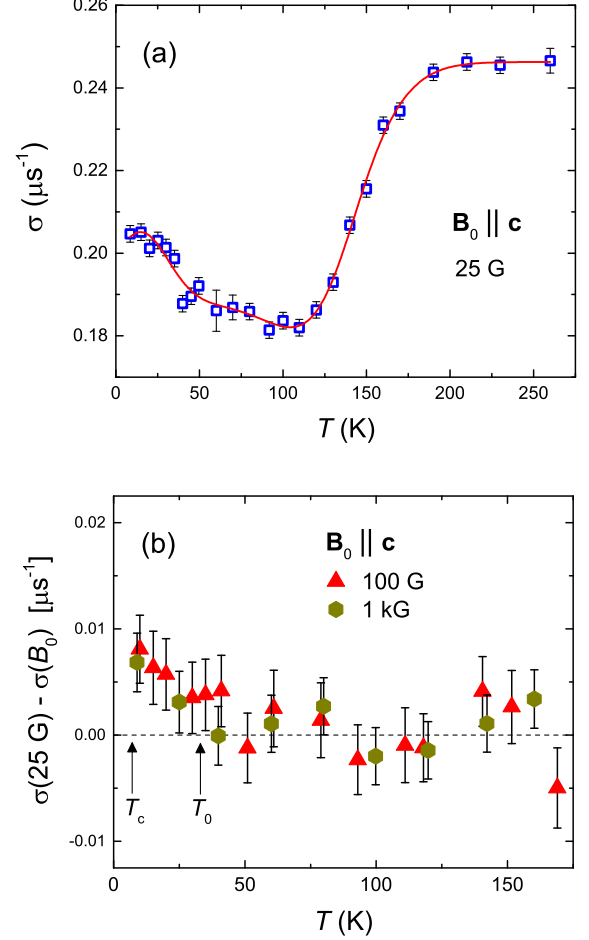


FIG. 3: (Color online) (a) Temperature dependence of the muon depolarization rate σ above T_c for a magnetic field of 25 G applied parallel to the c axis (This data is also shown in Fig. 2). The solid curve through the data points is a guide to the eye. (b) Difference between σ for $B_0 = 25$ G and 100 G, and for $B_0 = 25$ G and 1 kG. The solid curve from (a) was used to calculate these differences at temperatures where no 25 G data exist.

averaging over the distribution of fields it experiences during its lifetime as it moves from site to site (a situation analogous to motional narrowing of the line width in NMR). Above $T \sim 110$ K the increase of σ suggests that at these temperatures at least some of the μ^+ move fast enough to reach sites near defects within their various lifetimes. Consequently, the enhanced σ results from the muon ensemble sensing a broadened distribution of time-averaged magnetic fields. The plateau appearing above $T \sim 200$ K suggests that at these higher temperatures the μ^+ hop rate becomes very fast, such that most of the μ^+ reach the vicinity of a defect very early in their lifetime — where they presumably experience a broader distribution of nuclear dipole fields. The muon hop rate is not influenced by the applied magnetic field, and hence the

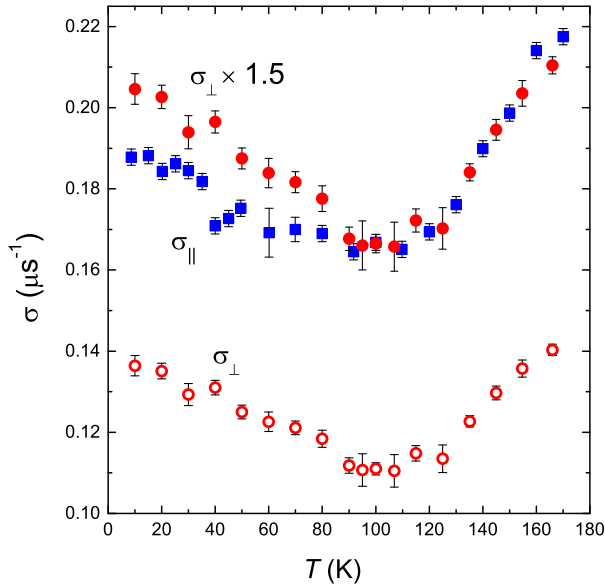


FIG. 4: (Color online) Temperature dependence of the muon depolarization rate above T_c for a magnetic field of $B_0 = 25$ G applied parallel (σ_{\parallel}) or perpendicular (σ_{\perp}) to the c axis. The solid red circles are the σ_{\perp} data multiplied by a scaling factor of 1.5.

behavior of σ as a function of temperature is more or less the same for all fields.

In actuality, below $T \sim T_0$ there is some difference between σ for $B_0 = 25$ G and the data for higher applied fields. While this is noticeable in Fig. 2, it is more obvious in a plot of the difference between σ values. As shown in Fig. 3(b), the difference between σ for $B_0 = 25$ G and data collected for $B_0 = 100$ G or 1 kG increases with decreasing temperature below $T \sim T_0$. Changes in the form of the ZF- μ SR signal are also observed below T_0 , where there is no \mathbf{B}_0 to affect the ^{93}Nb quantization axis.¹⁷ At $B_0 = 25$ G, where the ratio $\langle I_x^{\text{Nb}} \rangle / \langle I_z^{\text{Nb}} \rangle \sim \nu_Q / \nu_Z$ is quite large, the quantization axis for the ^{93}Nb nuclear spin states is also solely determined by the direction of the maximal EFG at the nuclear site. At all temperatures there are contributions to the net EFG at the ^{93}Nb nuclear site from the crystal lattice and the electric field directed radially away from the μ^+ . The onset of CDW order below T_0 introduces an additional contribution that rotates the direction of the maximal EFG, hence changing σ_{Nb} . Nevertheless, for this orientation of \mathbf{B}_0 the effect is quite weak.

Figure 4 shows the effect of changing the direction of the applied field to be perpendicular to the c axis ($\mathbf{B}_0 \perp \mathbf{c}$). To maintain the transverse-field geometry, this also requires changing the direction of $\mathbf{P}(0)$ to be parallel (rather than perpendicular) to the c axis. Due to the anisotropic nature of the dipolar interaction between the μ^+ and the host nuclei, the fitted values of σ are expected to show a dependence on the change in directions of \mathbf{B}_0

and $\mathbf{P}(0)$. In particular, the change in direction of \mathbf{B}_0 results in a change in the angles θ_i and θ_j in Eqs. (2) and (3), and the change in direction of $\mathbf{P}(0)$ corresponds to a change in the direction of the μ^+ spin. For $B_0 = 25$ G, the quantization axis for the μ^+ spin states rotates with \mathbf{B}_0 , but the quantization axis for the ^{93}Nb spin states determined solely by the net EFG does not. With the direction of the maximal EFG at the ^{93}Nb nuclear site fixed and continuing to define the direction of \mathbf{B}_0 as the z direction, the 90° rotation of \mathbf{B}_0 changes the ratio of $\langle I_x^{\text{Nb}} \rangle / \langle I_z^{\text{Nb}} \rangle$ in Eq. (3).

To see the effect on σ of changing the angle between \mathbf{B}_0 and the EFG associated with CDW order, we show the data for $\mathbf{B}_0 \perp \mathbf{c}$ (*i.e.* σ_{\perp}) in Fig. 4 multiplied by a scaling factor that eliminates the anisotropy in σ at high temperatures. Below $T \sim 90$ K there is a clear enhancement of the scaled σ_{\perp} data above σ_{\parallel} , indicating a change in the angle between the quantization axes of the ^{93}Nb nuclear and μ^+ spin states. This suggests that the μ^+ is sensitive to static CDW order up to temperatures nearly 3 times the CDW phase transition temperature T_0 — consistent with the STM study of Ref. 14, which as mentioned earlier shows nanometer-size regions of static CDW order in the vicinity of defects at the surface of the sample in the temperature range $T_0 < T < 3T_0$. The STM measurements demonstrate an increase of the correlation length of the CDW regions as the temperature is lowered toward T_0 . Assuming the same occurs in the bulk, with decreasing temperature a greater number of the mobile μ^+ encounter regions of CDW order during their lifetime.

IV. SUMMARY

In the present work we have demonstrated the sensitivity of TF- μ SR to static CDW order in the bulk of $2H\text{-NbSe}_2$. The results support early NMR findings, and recent STM measurements at the surface of $2H\text{-NbSe}_2$ showing the occurrence of nanodomains of static CDW order above T_0 near defects. It is shown that the μ^+ is mobile at temperatures above T_c , and may become trapped by defects during its lifetime. Above T_0 this mobility presumably allows a greater number of the implanted muons to experience the short-range CDW correlations.

Acknowledgments

We thank R.F. Kiefl for informative discussions and the staff of TRIUMF's Centre for Molecular and Materials Science for technical assistance. JES acknowledges support from the Canadian Institute for Advanced Research and the Natural Sciences and Engineering Research Council of Canada.

-
- ¹ J. Chang, E. Blackburn, A. T. Holmes, N. B. Christensen, J. Larsen, J. Mesot, R. Liang, D. A. Bonn, W. N. Hardy, A. Watenphul, M. V. Zimmermann, E. M. Forgan, and S. M. Hayden, *Nature Physics* **8**, 871-876 (2012).
 - ² G. Ghiringhelli, M. Le Tacon, M. Minola, S. Blanco-Canosa, C. Mazzoli, N. B. Brookes, G. M. De Luca, A. Frano, D. G. Hawthorn, F. He, T. Loew, M. Moretti Sala, D. C. Peets, M. Salluzzo, R. Sutarto, G. A. Sawatzky, E. Weschke, B. Keimer, and L. Braicovich, *Science* **337**, 821-825 (2012).
 - ³ R. Comin, A. Frano, M. M. Yee, Y. Yoshida, H. Eisaki, E. Schierle, E. Weschke, R. Sutarto, F. He, A. Soumyanarayanan, Y. He, M. Le Tacon, I. S. Elfimov, J. E. Hoffman, G. A. Sawatzky, B. Keimer, A. Damascelli, *Science* **343**, 390-392 (2014).
 - ⁴ E. H. da Silva Neto, P. Aynajian, A. Frano, R. Comin, E. Schierle, E. Weschke, A. Gyenis, J. Wen, J. Schneeloch, Z. Xu, S. Ono, G. Gu, M. Le Tacon, A. Yazdani, *Science* **343**, 393-396 (2014).
 - ⁵ S. Blanco-Canosa, A. Frano, E. Schierle, J. Porras, T. Loew, M. Minola, M. Bluschke, E. Weschke, B. Keimer, and M. Le Tacon, *Phys. Rev. B* **90**, 054513 (2014).
 - ⁶ M. Hübner, N. B. Christensen, A. T. Holmes, E. Blackburn, E. M. Forgan, Ruixing Liang, D. A. Bonn, W. N. Hardy, O. Gutowski, M. v. Zimmermann, S. M. Hayden, and J. Chang, *Phys. Rev. B* **90**, 054514 (2014).
 - ⁷ E. H. da Silva Neto, R. Comin, F. He, R. Sutarto, Y. Jiang, R. L. Greene, G. A. Sawatzky, and A. Damascelli, *Science* **347**, 282-285 (2015).
 - ⁸ S. V. Borisenko, A. A. Kordyuk, V. B. Zabolotnyy, D. S. Inosov, D. Evtushinsky, B. Büchner, A. N. Yaresko, A. Varykhalov, R. Follath, W. Eberhardt, L. Patthey, and H. Berger, *Phys. Rev. Lett.* **102**, 166402 (2009).
 - ⁹ J. A. Wilson, F. J. DiSalvo, and S. Mahajan, *Adv. Phys.* **24**, 117 (1975).
 - ¹⁰ J. A. R. Stiles and D. L. Williams, *J. Phys. C.: Solid State Phys.* **9**, 3941-3953 (1976).
 - ¹¹ K. Ghoshray, B. Pahari, A. Ghoshray, V. V. Eremin, V. A. Sirenko, and B. H. Suits, *J. Phys.: Condens. Matter* **21**, 155701 (2009).
 - ¹² C. Berthier, D. Jerome, and P. Molinie, *J. Phys. C.: Solid State Phys.* **11**, 797-814 (1978).
 - ¹³ M. Le Tacon, A. Bosak, S. M. Souliou, G. Dellea, T. Loew, R. Heid, K.-P. Bohnen, G. Ghiringhelli, M. Krisch, and B. Keimer, *Nature Physics* **10**, 52 (2014).
 - ¹⁴ C. J. Arguello, S. P. Chockalingam, E. P. Rosenthal, L. Zhao, C. Gutiérrez, J. H. Kang, W. C. Chung, R. M. Fernandes, S. Jia, A. J. Millis, R. J. Cava, and A. N. Pasupathy, *Phys. Rev. B* **89**, 235115 (2014).
 - ¹⁵ U. Chatterjee, J. Zhao, M. Iavarone, R. Di Capua, J. P. Castellan, G. Karapetrov, C. D. Malliakas, M. G. Kanatzidis, H. Claus, J. P. C. Ruff, F. Weber, J. van Wezel, J. C. Campuzano, R. Osborn, M. Randeria, N. Trivedi, M.R. Norman, and S. Rosenkranz, *Nature Communications* **6**, 6313 (2015).
 - ¹⁶ O. Hartmann, *Phys. Rev. Lett.* **39**, 832 (1977).
 - ¹⁷ W. Higemoto, K. Nagamine, S. Kuroda, and K. Takita, *Hyperfine Interactions* **120/121**, 591 (1999).
 - ¹⁸ F. D. Callaghan, M. Laulajainen, C. V. Kaiser, and J. E. Sonier, *Phys. Rev. Lett.* **95**, 197001 (2005).